Electrochimica Acta 473 (2024) 143494

Contents lists available at ScienceDirect

Electrochimica Acta

journal homepage: www.journals.elsevier.com/electrochimica-acta

Effects of operating temperature on Li-O_2 battery with ionic liquid-based binary electrolyte

Syed Shoaib Hassan Zaidi [a], Rajkumar Kore [b], Mark B. Shiflett [b], Xianglin Li [a,c,*]

[a] Department of Mechanical Engineering, University of Kansas, Lawrence, Kansas 66045, USA
[b] Department of Chemical and Petroleum Engineering, University of Kansas, Lawrence, Kansas 66045, USA
[c] Department of Mechanical Engineering and Materials Science, Washington University in St. Louis, St. Louis, MO 63130, USA

ARTICLE INFO

Keywords:
Lithium oxygen battery
Operating temperature
Ionic liquid
Binary electrolyte
Viscosity
Ionic conductivity

ABSTRACT

Awaiting a breakthrough, the Li-oxygen battery (LOB) is considered a promising candidate to meet the high energy demands in the future. Among various critical challenges which hamper its development, the mystery of the electrolyte with optimal properties remains unsolved to this day. In this study, we comprehensively investigated the effects of operating temperature (20C, 40 °C and 60 °C) on the electrochemical performance of LOBs incorporated with room temperature ionic liquid (RTIL) and organic solvent binary electrolyte. We designed and investigated 1-Ethyl-3-methylimidazolium bis(trifluoromethylsulfonyl)imide ([C_2C_1*im*][Tf_2N]) RTIL and dimethyl sulfoxide (DMSO) organic solvent at various volume ratios ((4:1), (1:1), (1:4)). Among the binary electrolytes, ([C_2C_1*im*][Tf_2N]/DMSO (1:4)) delivered the highest discharge capacities of 3.70 Ah g^{-1} (20 °C), 4.0 Ah g^{-1} (40 °C) and 3.65 Ah g^{-1} (60 °C) as compared with pure [C_2C_1im][Tf_2N] and DMSO. Cycling stability tests showed superior stability of the binary electrolyte ([C_2C_1*im*][Tf_2N]/DMSO (1:4)) irrespective of the operating temperature. From viscosity and ionic conductivity measurements (at 20–60 °C), [C_2C_1im][Tf_2N]/DMSO (1:4) exhibited the highest ionic conductivity and the lowest viscosity compared with other binary electrolytes (even with pure electrolytes) at any given temperature. Cyclic voltammetry (CV) tests revealed the highest reaction rates for [C_2C_1im][Tf_2N]/DMSO (1:4) binary electrolytes than pure electrolytes. The superior performance of [C_2C_1im][Tf_2N]/DMSO (1:4) binary electrolyte was ascribed to enhanced stability against reactive intermediate species during oxygen reduction reaction (ORR), increased ionic conductivity, low viscosity (comparable with organic electrolytes), improved oxygen solubility, and relatively low evaporation rates.

1. Introduction

The world is reeling from the devastating effects of climate change due to over consumption of fossil fuels. The state-of-the-art Li-ion battery (LIB) has brought a revolution to portable electronic devices, but its limited specific energy density restricts its application to meet the high energy demands of the automobile industry. Consequently, efforts were made to circumvent the limitations of LIBs by adopting better energy storage alternatives. Among them, rechargeable Li-O_2 battery (LOB) has been under the spotlight of the scientific community owing to its exceptionally high theoretical energy density (~3500 Wh kg^{-1} based on the mass of discharge product, Li_2O_2) which is an order of magnitude higher than LIB's [1–3].

The possible reaction mechanism for aprotic (non-aqueous) LOB is presented in eqs 1(a-c) [4,5]. It undergoes oxygen reduction reaction (ORR) and oxygen evolution reaction (OER) during discharge and charge cycle, respectively.

$$\textit{Anode}: 2\text{Li} \leftrightarrow 2\text{Li}^{+} + 2e^{-} \tag{1a}$$

$$\textit{Cathode}: 2\text{Li}^{+} + 2e^{-} + \text{O}_2 \leftrightarrow \text{Li}_2\text{O}_2 \tag{1b}$$

$$\textit{Overall}: 2\text{Li} + \text{O}_2 \leftrightarrow \text{Li}_2\text{O}_2 \quad E^{\circ} = 2.96V \tag{1c}$$

Ideally, as a result of discharge cycle, Li_2O_2 accumulates on the surface of porous cathode which disintegrates back to Li^+ and O_2 during charge cycle.

Abraham and Jiang reported the first non-aqueous electrolyte-based LOB, which eliminated the potential risk of side reactions in aqueous LOBs proposed earlier [6]. Since then, aprotic (non-aqueous) LOBs have garnered the focus of research due to their high reversibility [7].

* Corresponding author.
E-mail address: lxianglin@wustl.edu (X. Li).

https://doi.org/10.1016/j.electacta.2023.143494
Received 14 March 2023; Received in revised form 6 November 2023; Accepted 11 November 2023
Available online 13 November 2023

Nonetheless, the progress of rechargeable LOBs is stymied owing to the number of challenges its components present. Among various critical challenges, the choice of electrolyte has always been a bottleneck, impeding the breakthrough in the development of LOB [8]. The characteristics of an ideal electrolyte for LOB are (i) high ionic conductivity, (ii) low volatility, (iii) low viscosity, (iv) high oxygen solubility and diffusivity, (v) high electrochemical stability, and (vi) high chemical stability with the cell components and in the presence of highly reactive O_2^- produced during intermediate reaction [3,9].

Organic solvent-based electrolytes (carbonates, sulfones, amide, ethers, etc.) have been extensively studied in LOBs due to their low viscosities and superior mass transport properties. However, several reports in the literature reveal that organic solvents are chemically unstable in the presence of highly reactive reduced oxygen species, and they tend to degrade during the charge cycle due to high overvoltage. Consequently, undesired and irreversible discharge products accumulate on the porous cathode leading to the shorter life of the battery [10–12]. Additionally, organic solvents' volatile and flammable nature poses safety issues as the battery electrolyte. Room temperature ionic liquids (RTILs) have been investigated as a potential electrolyte solvent in LOBs for the past several years. Unlike oragnic solvents, they possess unique properties, including nonvolatility, nonflammability, high electrochemical, chemical and thermal stability [13]. The one major drawback of these electrolytes is their intrinsically high viscosity and consequently high mass transfer resistance. Slow mass transfer rates restrict their application to low current density applications [14].

Currently, no electrolyte could be regarded as an ideal electrolyte. Nonetheless, efforts have been made to improve electrolyte properties by blending two or more miscible electrolyte solvents. The blending of IL and organic solvent in an optimized ratio can combine the remarkable properties of ILs, including low vapor pressure, high thermal and electrochemical stability, and superior transport properties of organic solvents. Zeng et al. incorporated 1-ethyl-3-methylimidazolium bis (trifluoromethylsulfonyl)imide $[C_2C_1im][Tf_2N]$ (80 wt%) and DMSO (20 wt%) binary electrolytes and improved the cycling stability of LOB from 58 cycles to 65 cycles at 0.1 mA cm^{-2} utilizing Co_3O_4 catalyzed cathode [15]. Similarly, Knipping and coworkers achieved higher discharge capacity (7,618 vs. 5651 mAh g^{-1}) and lower polarization (1.06 vs 1.43 V) with $[C_2C_1im][Tf_2N]$ and DMSO (70/30 wt%) mixed electrolyte as compared with pure DMSO electrolyte [16]. Mohammad et al. employed 1-ethyl-3-methylimidazolium tetrafluoroborate ($[C_2C_1\mathit{im}][BF_4]$) and DMSO (25%/75%) mixture with MoS_2 cathode and protected Li anode and achieved long cycle life of 700 cycles (500 mAh g^{-1} at 500 mA g^{-1}) in an air-like atmosphere [17]. Ferrari and coworkers demonstrated superior electrochemical stability, and ionic conductivity of *N*-methoxyethyl-*N*-methylpyrrolidinium bis (trifluoromethanesulfonyl)-imide ($PYR_{1,2O1}$TFSI) (50 vol%) and tetraethylene glycol dimethyl ether (TEGDME) (50 vol%) blended electrolyte and achieved a high discharge capacity of 4000 mAh g^{-1} [18]. Asim and Chuan combined 1-butyl-1-methyl-pyrrolidinium bis(trifluoromethylsulfonyl)imide ($[BMP][Tf_2N]$) and DMSO and observed higher reaction rates in mixture electrolytes as compared with neat solvents [19]. Laura et al. reported improved reversibility and ionic conductivity (0.87 to 3.5 mS cm^{-1}) using a N-methyl-(n-butyl) pyrrolidinium bis(trifluoromethane sulfonyl) imide (PYR_{14}TFSI) and TEGDME (1:1 v/v) binary electrolyte [20].

The aforementioned studies have tuned the physiochemical properties of the electrolyte by combining IL and organic solvents and investigated the battery performance at room temperature. To the best of our knowledge, very limited studies have taken into account the effect of operating temperatures, in particular with blended electrolytes in LOBs. Some reports in the literature focused on the effects of operating temperature on either organic solvent [21,22] or RTIL [23–27] in LOBs. Herein, we present a comprehensive experimental investigation of the impact of operating temperature on the electrochemical performance of RTIL-organic electrolyte-based LOB. We combined the effect of operating temperature and blending of IL and organic solvent in order to tune the physiochemical properties of the resulting electrolyte. For RTIL, we selected 1-ethyl-3-methylimidazolium bis(trifluoromethylsulfonyl) imide ($[C_2C_1\mathit{im}][Tf_2N]$, will be referred as IL in this paper) due to its relatively low viscosity as compared with other RTILs, high thermal and electrochemical stability, and superior ionic conductivity [25]. The chemical structures of cation and anion are illustrated in Fig. S1 in supplementary information. Dimethyl sulfoxide (DMSO) was incorporated as an organic solvent in this study. We measured viscosity and effective ionic conductivity of various combinations of IL and DMSO (with 0.5 M Lithium bis(trifluoromethane)sulfonimide-LiTFSI) including (4:1), (1:1), (1:4) by vol% at different operating temperatures (20 °C, 40 °C and 60 °C). Owing to the superior battery performance of 0.5 M LiTFSI-IL/DMSO (1:4) binary electrolyte among other electrolyte mixtures, it was employed for further electrochemical tests. Galvanostatic deep discharge tests and cycling stability tests were conducted at various temperatures. Cyclic voltammetry tests were conducted to study the impact of temperature on reaction rates. IL/DMSO (1:4) binary electrolytes achieved the highest discharge capacity and cycling stability as compared with neat electrolytes at any given operating temperature.

2. Experimental

2.1. Electrolytes preparation

Ionic liquid, 1-ethyl-3-methylimidazolium bis(trifluoromethylsulfonyl)imide was purchased from IoLiTec Gmbh (assay, 99 wt%, CAS no. 174,899–82–2, Lot and filling Code no. T006 × 98.1-IL-0023) and dried further before use. The IL was dried and degassed at 25 °C under a high vacuum (10^{-9} MPa) for 24−48 h to remove water and volatile impurities. Commercially available organic solvent Dimethyl sulfoxide (DMSO, anhydrous>99.9%) was utilized as a cosolvent. Lithium Bis(trifluoromethane)sulfonimide (LiTFSI, 99.95%) was exploited as Li salt to make a 0.5 M concentration solution with both solvents and their binary combinations. Three binary electrolyte mixtures (IL/DMSO) in volume ratios of (4:1), (1:1), (1:4) were prepared. All commercial materials except the IL were purchased from Sigma-Aldrich and used as received in this study. All materials were opened and stored in Ar-filled glovebox with H_2O and O_2 levels <0.1 ppm.

2.2. Physiochemical properties measurements

Brookfield DV-II+Pro-Viscometer was used to measure the viscosities of neat solvents and their various electrolyte mixtures at 20 °C (RT), 40 °C, and 60 °C. Galvanostatic EIS measurements were conducted with the SS||SS symmetric cells to measure the effective ionic conductivity of the electrolyte material in the glass fiber separator material under compression using Biologic SP-150 potentiostat. Anodic electrochemical stability windows (ESW) of pure and binary electrolytes (at RT) were determined by linear sweep voltage (LSV) technique at a scan rate of 10 mV s^{-1}. Evaporation rates of electrolytes were measured for 24 h at 20 °C, 40 °C and 60 °C in glovebox in order to eliminate the error from moisture.

2.3. Oxygen cathode preparation

Vulcan XC 72R purchased from Fuel Cell Store was used as the active material coated on carbon cloth. Vulcan XC 72R was mixed with polytetrafluoroethylene (PTFE) binder (70:30 wt% ratio) in isopropyl alcohol (IPA) and water solution (70:30 vol% ratio). The mixture was then sonicated in a Branson bath sonicator for 3 h to combine all components well. The prepared slurry was blade coated on 1071 HCB plain carbon cloth. The coated substrate was then dried for 24 h at RT (20 °C), followed by heat treatment in a SentroTech furnace at 350 °C for 30 min. The electrodes were punched in 1.27 cm diameter for battery assembly.

Table 1
Viscosity measurements of neat solvents ([C_2C_1*im*][Tf_2N], DMSO), [C_2C_1im][T*f*$_2$N], DMSO and various binary combinations with 0.5 M LiTFSI salt concentration conducted at 20 °C, 40 °C, and 60 °C. The calculated activation energy (E_a) of viscosity's temperature dependence is also reported in the table.

Temperature (°C)	Viscosity (η/mPa s)						
	Pure IL	0.5 M LiTFSI-IL	0.5 M LiTFSI-IL/DMSO (4:1)	0.5 M LiTFSI-IL/DMSO (1:1)	0.5 M LiTFSI-IL/DMSO (1:4)	0.5 M LiTFSI-DMSO	Pure DMSO
20	34.1	47.5	27.6	9.18	4.28	3.02	2.11
40	17.1	22	14.5	6.16	2.65	1.9	1.37
60	10	12.3	8.14	3.37	1.75	1.29	0.95
E_a (kJ moL^{-1})	24.9 ± 0.74	27.4 ± 1.04	24.74 ± 0.27	20.18 ± 3.24	18.13 ± 0.01	17.25 ± 0.16	16.18 ± 0.08

The measured carbon loading for each electrode of area 1.27 cm^2 was 1.3 ± 0.15 mg cm^{-2}.

2.4. Battery assembly

The battery was assembled in an argon-filled Mikrouna glovebox with O_2 and H_2O concentrations maintained below 0.1 ppm. The as-prepared oxygen cathode was first placed in the battery frame. It was stacked by an electrolyte-soaked Whatman glass fiber separator (GF/C, 1822–021) with a diameter of 1.58 cm. Each battery utilized 90 μL of electrolyte. A Li chip (0.25 mm thick) with 1.27 cm^2 was placed on top of the separator, which served as the anode. The battery was screwed appropriately to avoid leakage and exposure to the atmosphere.

2.5. Electrochemical measurements

The assembled battery was supplied continuously with 99.99% pure oxygen at 1 atm pressure. The battery was purged with oxygen at open circuit voltage (OCV) for at least 1 h to ensure the complete removal of argon from the electrode assembly. In order to study the impact of operating temperature on ORR and OER, cyclic voltammetry (CV) tests were conducted using Biologic SP-150 potentiostat at the scan rate of 0.1 mV s^{-1}. Galvanostatic discharge/charge capacity tests were performed on an 8-channel Neware BTS8.0 battery cycler at three different temperatures (20 °C, 40 °C, and 60 °C). Cycling stability tests were conducted with the curtailed capacity of 1.0 Ah g^{-1}. All specific capacity tests were carried out at 0.1 mA cm^{-2} current density. The discharge and charge cutoff voltages used were 2.0 V and 4.5 V, respectively, for both CV and discharge/charge capacity tests. All deep discharge and cycling stability tests were repeated three times.

2.6. Material characterization

In order to investigate the influence of operating temperatures on the morphology of discharge product (Li_2O_2), deep discharged cathodes using a binary electrolyte, were analyzed under Hitachi SU8230 Field Emission Scanning Electron Microscope (SEM). The composition of discharge product was examined by PHI 5000 Versa Probe II X-ray Photoelectron Spectroscopy (XPS) analysis. Moreover, the presence of Li_2O_2 was also confirmed by Raman Spectroscopy. For this purpose, the fresh and discharged electrodes were examined under Horiba Jobin Yvon LabRam ARAMIS Micro-Raman Microscope using 785 nm laser excitation.

3. Results and discussion

3.1. Physical properties

3.1.1. Viscosity

The viscosity of an electrolyte is one of the critical parameters that determine battery performance. It profoundly impacts electrolyte's transport properties [34]. In LOBs, the gaseous oxygen is supplied from outside to react with Li^+ ions to form the discharge product i.e., Li_2O_2. The diffusivity of ions is critical to transport to electrochemically active sites of porous cathode and achieve high discharge capacity. The diffusivity of electrochemical species is inversely related to the viscosity of electrolyte [4]. Table 1 shows the viscosity measurements of pure solvents (IL and DMSO) and the various combinations with 0.5 M LiTFSI salt concentration at three different temperatures, including 20 °C (RT), 40 °C, and 60 °C. 0.5 M LiTFSI/IL shows the highest viscosity of all the electrolytes at any given temperature. This is intuitive as the RTILs exhibit high viscosity intrinsically as compared with organic solvents. On the contrary, the pure DMSO, an organic solvent, displays the lowest viscosity. The viscosities of pure solvents are in good agreement with the published data [28,29]. The effect of salt concentration on the viscosity of electrolytes is also substantial. Especially, the viscosity of pure IL is increased by ~40% when measured with 0.5 M LiTFSI salt concentration. Overall, the viscosity decreases with increasing temperature regardless of electrolyte (with or without salt).

These results indicate that electrolyte viscosity is strongly contingent on the operating temperature. All electrolytes and their binary systems follow the Andrade equation (Eq. (2)), which is analogous to the

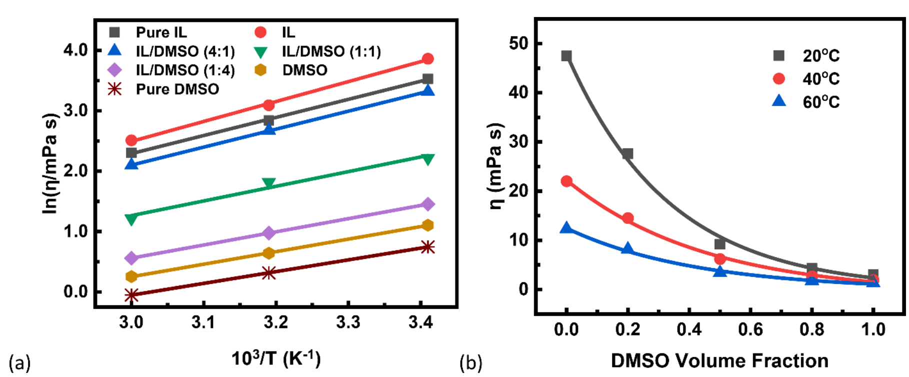

Fig. 1. **(a)** Arrhenius plots for viscosities of various electrolytes and **(b)** Variation of viscosity of binary electrolytes with DMSO volume fraction at 20 °C, 40 °C, and 60 °C.

Table 2
Effective ionic conductivity measurements of $[C_2C_1im][Tf_2N]$, DMSO and various binary combinations with 0.5 M LiTFSI salt concentration conducted at 20 °C, 40 °C, and 60 °C.

Electrolyte	Effective Ionic Conductivity (σ/mS cm^{-1})		
	T = 20 °C	T = 40 °C	T = 60 °C
IL	5.59	8.25	10.72
IL/DMSO (4:1)	6.43	9.12	11.83
IL/DMSO (1:1)	8.87	11.52	14.12
IL/DMSO (1:4)	10.34	13.00	15.09
DMSO	7.59	10.10	12.75

Arrhenius equation [30].

$$\eta = \eta^{o}\exp\left[\frac{E_a}{RT}\right] \tag{2}$$

Here, η^{o} is a constant, E_a is the activation energy, R denotes the universal gas constant, and T represents the temperature.

Fig. 1a shows the Arrhenius plot of the viscosity change of electrolytes with T^{-1}. The measured viscosities are a good fit with the Arrhenius model. From these Arrhenius plots, the activation energies of these electrolytes were calculated (as shown in Table 1). The activation energies of pure solvents are in good agreement with the previous reports [31].

The volume fraction of DMSO also has a significant impact on RTIL-organic solvent binary systems. Table 1 shows that the viscosity decreases with the increase in DMSO volume fraction regardless of temperature. When viscosities of binary systems were plotted against DMSO volume fraction, an exponential trend emerged, as shown in Fig. 1b. The exponential decrease in viscosities with DMSO volume fraction also refers to an exponential increase in diffusivity of electrochemical species. This behavior is explained by the classical Stokes-Einstein equation (Eq. (3) [32,33].

$$D = \frac{kT}{c\pi\eta a} \tag{3}$$

Here, k is Boltzmann's constant, a is the effective radius of diffusing species, c is a constant that depends on slip or no-slip conditions. An increase in temperature and volume fraction of DMSO greatly reduces the viscosity of mixture electrolytes and consequently enhances the diffusivity of ions in the electrolyte.

3.1.2. Effective ionic conductivity

The effective ionic conductivity (σ_{eff}) of an electrolyte is another important parameter that affects the battery's performance. Effective ionic conductivity of an electrolyte in general, is affected by various factors, including temperature [34], viscosity [35], salt concentration [36], state of electrolyte [37] and type of electrolyte [38]. We investigated the effective ionic conductivity of various combinations of IL/DMSO binary systems with 0.5 M LiTFSI salt concentration at different operating temperatures (20 °C, 40 °C and 60 °C). Galvanostatic EIS measurements were conducted with the SS||SS symmetric cells to measure the effective ionic conductivity of the electrolyte material in the glass fiber separator material under compression. It is worth mentioning that the amount of pressure applied to the electrodes while assembling the battery may have significant impact on the measurements. Consequently, all tests were repeated three times in order to achieve consistent results. EIS plotted as Nyquist plots and equivalent circuit model (ECM) are shown in Fig. S2 in the supporting information. R1 represents the ohmic resistance of the electrolyte obtained from the high-frequency intercept of the fitted EIS spectrum on the real axis. σ_{eff} is then calculated using the following equation [15]:

$$\sigma_{eff} = \frac{t}{A \times R_1} \tag{4}$$

where t and A represent the thickness and area of the separator, respectively.

Table 2 shows the σ_{eff} measurements of various combinations of IL-DMSO binary systems at multiple temperatures. Effective ionic conductivity of any given electrolyte increases with temperature. This trend was expected as the increase in temperature caused a decrease in viscosity which increases the mobility of charged species and consequently effective ionic conductivity. Fig. 2a shows the Arrhenius plot of ionic conductivities and T^{-1}. The data fits well with the Arrhenius model and depicts the dependency of the effective ionic conductivity of the electrolyte on temperature.

It is interesting to note that the increase in effective ionic conductivity from pure IL electrolyte to IL/DMSO (1:4) at RT is more conspicuous than at elevated temperatures. Effective ionic conductivity increased by 85% at RT. However, it only increased by 40% at 60 °C. This behavior could be explained in terms of difference in their viscosities at two different temperatures. As mentioned in previous section, the difference in viscosities of pure IL and IL/DMSO (1:4) electrolytes at RT was 44.5 mPa s.

However, at 60 °C, the difference in their viscosities shrank to mere 11 mPa s. This implies that effective ionic conductivity is a strong function of viscosity. Nonetheless, the increase in effective ionic conductivity is not proportional to decrease in viscosity. Ionic conductivity and viscosity are correlated by Walden's rule which is as follows [39, 40]:

$$\Lambda\eta^{\alpha} = C \tag{5}$$

Here, Λ, η, α, and C represent molar conductivity, viscosity, slope of the Walden plot and temperature-dependent constant, respectively. The molar conductivity is calculated by the following equation:

$$\Lambda = \frac{\sigma}{c} \tag{6}$$

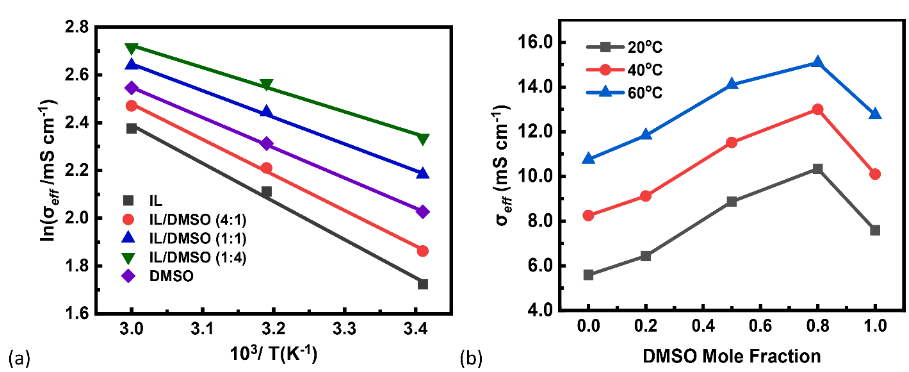

Fig. 2. **(a)** Arrhenius plots for effective ionic conductivities of various electrolytes and **(b)** Variation of effective ionic conductivities of binary electrolytes with DMSO volume fraction at 20 °C, 40 °C and 60 °C.

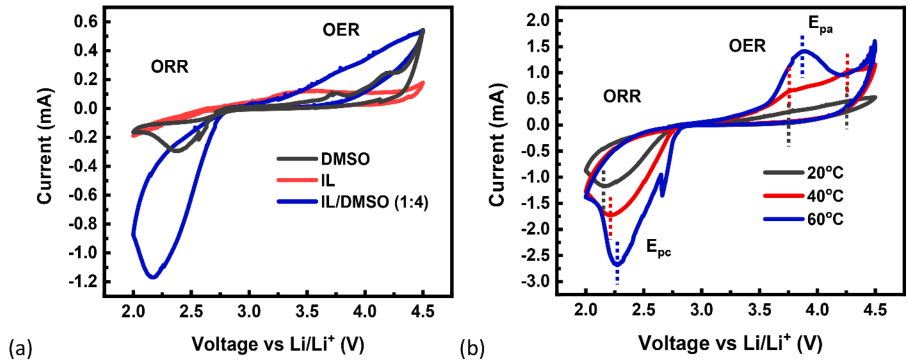

Fig. 3. (a) Comparison of CV profiles of $[C_2C_1im][Tf_2N]$, DMSO and $[C_2C_1im][Tf_2N]$/DMSO (1:4) with 0.5 M LiTFSI salt concentration solution at 20 °C (RT) **(b)** Comparison of CV profiles of 0.5 M LiTFSI-$[C_2C_1im][Tf_2N]$/DMSO (1:4) binary electrolyte at 20 °C, 40 °C and 60 °C. All tests were conducted at a scan rate of 0.1 mV s^{-1}.

Here, σ and c represents ionic conductivity and concentration of IL in mixture. Lopes and coworkers have shown that binary mixtures of IL and polar molecular solvents fairly fits Walden plot. This indicates that the conductivity of system is primarily governed by ion migration according to Stokes-Einstein equation and it's mainly determined by viscosity of system [39].

At the molecular level, effective ionic conductivity of an electrolyte depends on charge density and mobility of charge carriers. ILs exhibit higher charge density and latter is a strong function of bulk viscosity. Pure IL comprises of a continuous network of free ions (which contribute towards the ionic conductivity) and ion pairs. Initially, with the incorporation of polar solvent to the IL, effective ionic conductivity increases which could be ascribed to decreased viscosity and increased ion dissociation i.e., the clusters of interacting ions disintegrate and become free ions. This dissociation of ions gradually increases with the fraction of organic solvent until it reaches the state of infinite dilution when all charged species become free ions. This leads to the enhancement in effective ionic conductivity of IL-organic solvent mixture [41].

Fig. 2b shows the variation of σ_{eff} with the volume fraction of DMSO. The binary system with 80% DMSO exhibits the highest effective ionic conductivity. This could be attributed to the high degree of ion dissociation and reduced viscosity. The sharpe decrease in effective ionic conductivity with DMSO could be attributed to the decrease in number of charge carriers owing to the absence of IL. This effective ionic conductivity behavior for another RTIL-organic solvent binary system has been reported in the literature [15,16,30].

3.2. *Battery performance*

3.2.1. *Reaction mechanism*

The high electrochemical stability of RTILs is one of their distinguished properties that can improve battery cycle life. In LOB, the stability of electrolytes in the presence of nucleophilic superoxide radical (O_2^-) is significant. Without Li salt, the RTIL cation interacts with $O_2^-$and stabilizes it. The addition of Li salt introduces Li^+ ions in the solution. Owing to the smaller size and high charge density, Li^+ ions are hard acids in organic and IL solvents. Conversely, bulky RTIL cations with low charge density are soft acids. During the reduction reaction, with the generation of O_2^-, both cations compete to interact with it. Li^+ ions promote the disproportionation of O_2^- to peroxide (O_2^{-2}), as shown in reaction (8–9) [42,43]. In IL/DMSO binary electrolytes, high donor number (DN) of DMSO reduces the acidity of Li^+ ions which allows RTIL cations to interact with O_2^- more effectively (reaction 7) [44]. Following is the possible ORR and OER mechanism in IL/DMSO mixture [44–46].

Cathodic Reaction:

$$RTIL^+ + O_2 + e^- \rightarrow RTIL^+\text{—} O_2^- \quad (7)$$

$$Li^+ + O_2 + e^- \rightarrow LiO_2 \quad (8)$$

$$2LiO_2 \rightarrow Li_2O_2 + O_2 \quad (9)$$

$$LiO_2 + Li^+ + e^- \rightarrow Li_2O_2 \quad (10)$$

Anodic Reaction:

$$RTIL^+\text{—} O_2^- \rightarrow RTIL^+ + O_2 + e^- \quad (11)$$

$$Li_2O_2 \rightarrow 2Li^+ + O_2 + 2e^- \quad (12)$$

ORR and OER of neat electrolytes and IL/DMSO (1:4) binary electrolytes were investigated in LOB assembly using the cyclic voltammetry (CV) technique. Fig. 3a compares the CV curves obtained using three electrolytes at RT. The cathodic and anodic peaks refer to ORR and OER, respectively. Binary electrolytes achieved the highest current peaks, followed by DMSO and IL. The enhanced CV response of blended electrolytes could be ascribed to increased oxygen solubility and mass transport properties as compared with DMSO and IL, respectively [19]. When mixed electrolyte was subjected to elevated temperatures (Fig. 3b), the ORR rate increased substantially with temperature. Furthermore, with the rise in operating temperature, the cathodic current peaks (E_{pc}) shifted towards more positive potential. At 20 °C, 40 °C and 60 °C, the E_{pc} appeared at 2.15 V, 2.21 V and 2.28 V, respectively. This is attributed to the enhanced mass transfer properties of blended electrolyte with temperature, as illustrated in previous sections. The appearance of a single peak depicts the formation of Li_2O_2 by disproportionation or electrochemical reduction of LiO_2 (reaction 8–10). The oxidation peak current density was also influenced by temperature. As the temperature increases, the anodic peak (E_{pa}) becomes more pronounced. The OER followed the reaction pathway as described in reactions 11–12. It is noteworthy that at 20 °C and 40 °C, two E_{pa} emerged. However only one prominent E_{pa} appeared at 60 °C. The two anodic peaks can be ascribed to the reoxidation of Li_2O_2 and bulk Li_2O_2 at lower (~3.76 V) and higher (~4.25 V) potentials, respectively. The enhanced ORR and OER activity with temperature was also reported by Monaco and coworkers [47].

The EIS measurements of binary electrolyte-based LOB were conducted at OCV and various operating temperatures. Fig. S3 (a) shows the Nyquist plots of mixed electrolyte at 20 °C, 40 °C and 60 °C. The equivalent circuit model (ECM) is shown in Fig. S3 (b). Here, R1, R2, Q2 and W3 represents ohmic resistance, charge transfer resistance, constant phase element and Warburg constant, respectively. Ohmic resistance is calculated by high-frequency intercept at real axis which has negligible effect of temperature. However, the charge transfer resistance substantially decreased when temperature increased from 20 °C to 60 °C. At 20 °C, 40 °C and 60 °C, the charge transfer resistance was obtained as 123.4Ω, 46.17 Ω and 9.87 Ω, respectively. The drastic improvement in charge transfer rate with temperature also confirmed the enhanced electrochemical activity, as illustrated in CV tests.

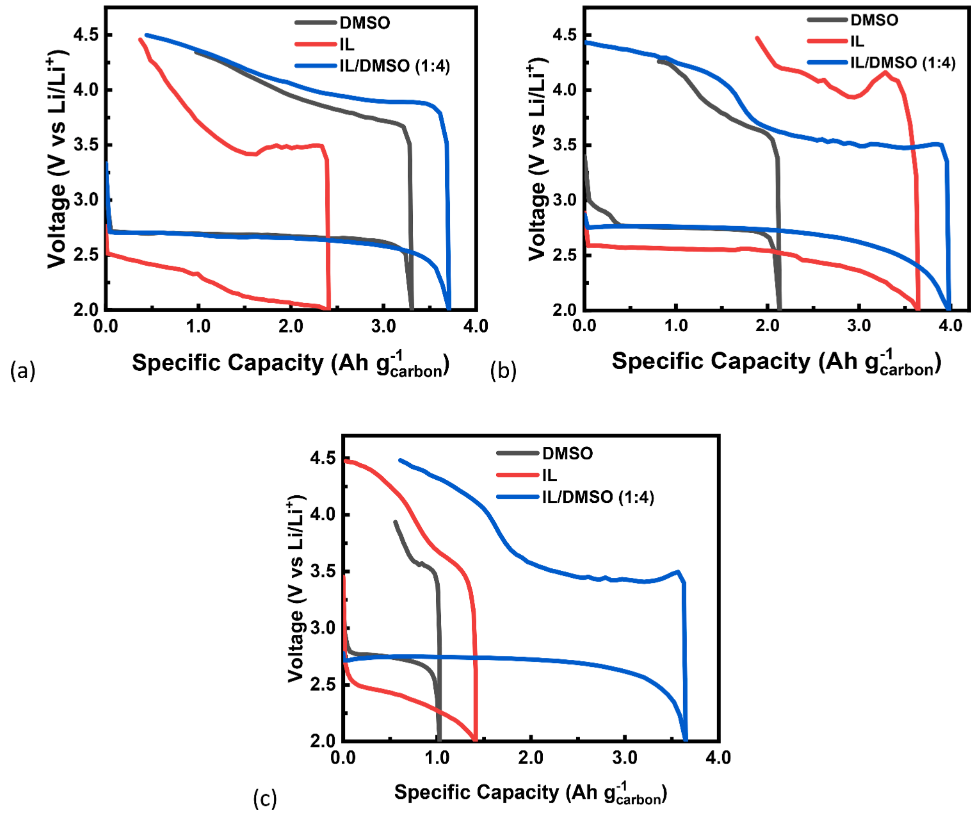

Fig. 4. Comparison of maximum discharge/charge capacity plot with $[C_2C_1im][Tf_2N]$, DMSO and $[C_2C_1im][Tf_2N]$/DMSO (1:4) prepared with 0.5 M LiTFSI salt concentration at **(a)** RT (20 °C) **(b)** 40 °C **(c)** 60 °C at a current density of 0.1 mA cm^{-2}.

3.2.2. Deep discharge tests

We investigated LOB performance with IL and DMSO and their various binary mixtures including IL/DMSO (4:1) (0.36 Ah g^{-1}), IL/DMSO (1:1) (2.05 Ah g^{-1}), IL/DMSO (1:4) (3.70 Ah g^{-1}) at 20°C (Figure S4 in supplementary information). IL/DMSO (1:4) outperforms other binary systems owing to its optimal properties, including low viscosity comparable with organic electrolyte and the highest ionic conductivity. Moreover, in order to improve the mass transport properties of a binary system significantly (comparable with organic solvent), at least 80 vol% of organic solvent should be added to IL [32]. We chose this IL-DMSO combination for further LOB testing. The anodic ESWs of pure IL, DMSO and IL/DMSO (1:4) electrolytes were determined at RT by scanning voltage from open circuit voltage (OCV) to 6 V in the absence of O_2. Fig. S5 shows the comparison of anodic ESWs of three electrolytes. The degradation of DMSO started well before 4.5 V. The addition of IL to DMSO extended its anodic ESW to >4.6 V. Intuitively, IL demonstrated widest anodic ESW, extended to >5.5 V. This behavior of binary electrolyte agrees well with the previous reports in literature [48,49]. Fig. 4 compares the maximum specific discharge/charge capacity profiles of three electrolyte systems at three different operating temperatures, including 20 °C (RT), 40 °C and 60 °C. Regardless of operating temperatures, IL/DMSO (1:4) displays superior performance as compared to pure electrolytes. At RT (Fig. 4a), the mixture electrolyte yields the highest discharge capacity (3.70 Ah g^{-1}, 4.28 mAh cm^{-2}) followed by DMSO (3.23 Ah g^{-1}, 3.97 mAh cm^{-2}) and IL (2.40 Ah g^{-1}, 3.23 mAh cm^{-2}). The superior performance of the binary electrolyte can be ascribed to its higher ionic conductivity and lower viscosity (comparable with DMSO). Moreover, IL (3.9 mM cm^{-1} [15]) exhibits much higher oxygen solubility as compared with DMSO (1.8 mM cm^{-1} [19]). Adding a small volume fraction of IL results in increased oxygen solubility of binary electrolytes without much compromise on viscosity and mass transport properties. DMSO trails behind binary electrolyte but still achieved a much higher discharge capacity than IL. This could be attributed to its much lower viscosity (enhanced diffusivity) and higher ionic conductivity than IL. The performance difference is more pronounced between DMSO and IL than between DMSO and binary electrolyte. This shows that the viscosity of electrolytes is a dominant factor that affects the LOB performance at RT.

At 40 °C (Fig. 4b), the binary electrolyte yields the highest discharge capacity (~4.0 Ah g^{-1}, 5.6 mAh cm^{-2}) followed by IL (3.64 Ah g^{-1}, 4.5 mAh cm^{-2}) and DMSO (2.13 Ah g^{-1}, 3.15 mAh cm^{-2}). Binary electrolyte displays moderate improvement in specific discharge capacity (~8% increase) when subjected to higher operating temperature. This could be attributed to enhanced mass transfer and ionic conductivity. On the other hand, the specific discharge capacity of IL improved dramatically (by ~52%) at 40°C. The viscosity of IL decreased substantially at 40°C (22.0 versus 47.5 mPa s). As discussed in the previous section, the diffusivity of ions increases at high temperatures due to low viscosity, which could be the reason for the high discharge capacity. Unlike binary electrolyte and IL, the specific discharge capacity of DMSO plummeted from 3.64 Ah g^{-1} to 2.13 Ah g^{-1} at a higher temperature. Although, like the other two electrolytes, the viscosity of DMSO decreases at 40 °C, the solubility of oxygen decreases with temperature as well [50,51]. DMSO already exhibits the lowest oxygen solubility among other electrolytes; an increase in temperature would further decrease the oxygen solubility. Additionally, another important parameter, solvent volatility, has rarely been highlighted and investigated when electrolyte performance in LOBs is under consideration. Since LOBs and other metal-air batteries are open systems as opposed to Li-ion batteries, the evaporation of electrolytes poses a great challenge. The loss of electrolyte can significantly impact LOB performance, especially when subjected to higher temperatures [52]. We investigated evaporation rates of IL, DMSO, and binary electrolytes at all three temperatures (Table S1 and Fig. S6 in the Supporting Information). DMSO exhibits highest evaporation rates followed by binary electrolyte and IL. This behavior was expected as RTILs possess the innate property of non-volatility and their incorporation in

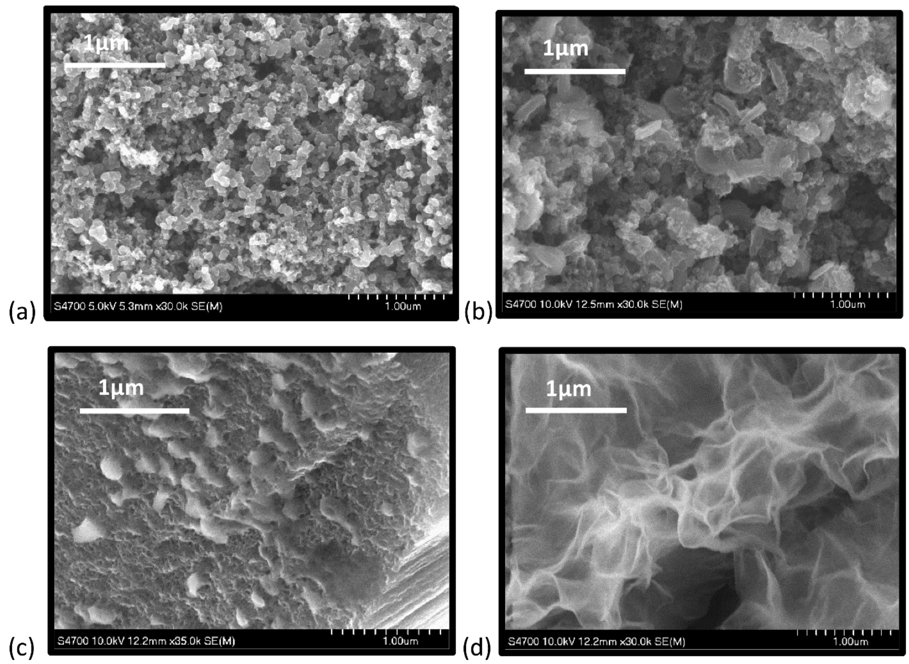

Fig. 5. SEM images show **(a)** pristine Vulcan XC and the evolution of Li_2O_2 morphology in LOB cathode discharged to the fixed capacity of 1.0 Ah g^{-1} with 0.5 M LiTFSI-[C_2C_1*im*][Tf_2N]/DMSO (1:4) at **(b)** RT (20 °C) **(c)** 40 °C **(d)** 60 °C.

organic solvents improve volatility as well, as demonstarted by binary electrolyte in this study.

Fig. 4c shows the discharge/charge profiles at 60 °C. The binary electrolyte outperforms its counterparts by yielding the highest specific discharge capacity, i.e., 3.65 Ah g^{-1}. IL and DMSO yield discharge capacities of 1.41 Ah g^{-1} and 1.02 Ah g^{-1}, respectively. The areal capacities for binary electrolytes, IL and DMSO were calculated as 5.08 mAh cm^{-2}, 1.97 mAh cm^{-2} and 1.5 mAh cm^{-2}, respectively. The overall discharge capacity decreases for all three electrolytes, nonetheless, the effect of temperature is more conspicuous in pure electrolytes.

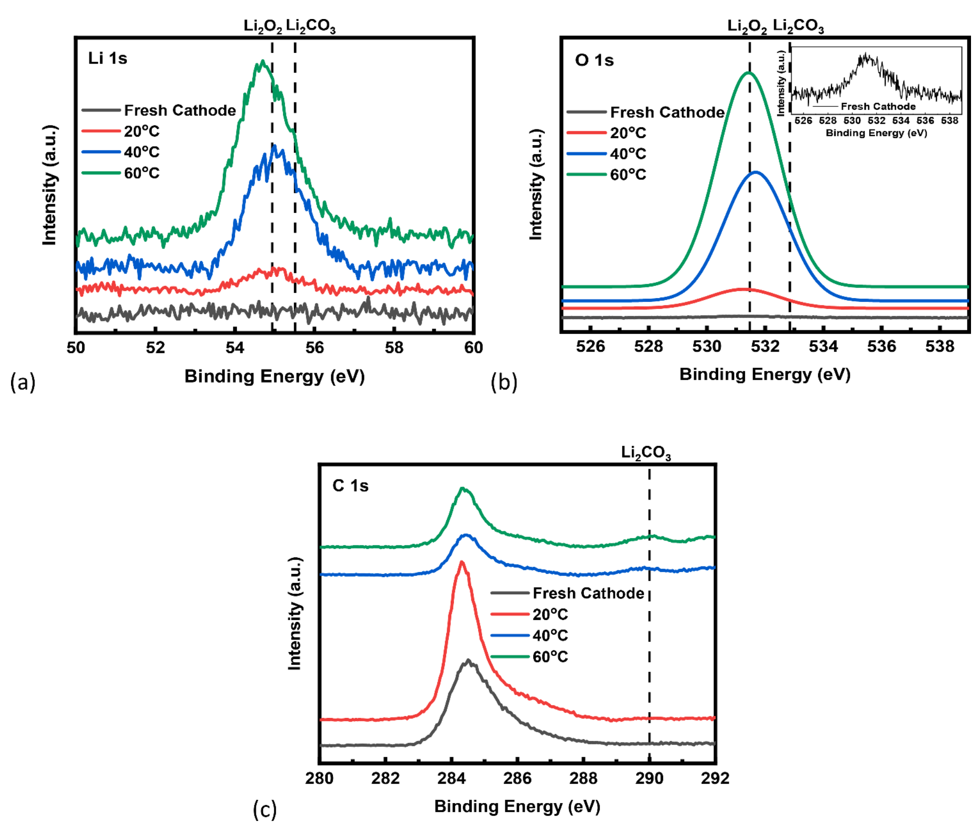

Fig. 6. XPS profiles of LOB cathode discharged to the fixed capacity of 1.0 Ah g^{-1} with 0.5 M LiTFSI-[C_2C_1*im*][Tf_2N]/DMSO (1:4) binary electrolyte at 20 °C, 40 °C, and 60 °C. The figure shows (a) Li 1 s, (b) O 1 s; inset: fresh cathode spectrum and (c) C 1 s spectra.

Table 3
Binding energies obtained from XPS analysis for Li_2O_2 in Li 1 s and O 1 s spectra at various temperatures.

Li_2O_2 Binding Energy (eV)		
Temperature (°C)	Li 1s	O 1s
20	54.90	531.26
40	54.95	531.67
60	54.72	531.42

Especially for IL, the improvement in discharge capacity when operating temperature increases from RT to 40 °C followed by a decline in performance at 60 °C was also reported elsewhere [53]. Although the mass transfer rate ameliorated further when the temperature increased to 60 °C, the deterioration of discharge capacity can be ascribed to the steep rate of evaporation for DMSO, degradation of IL, and an overall decrease in oxygen solubility for all electrolytes. The binary electrolyte maintained a higher discharge capacity even at 60 °C, comparable with the one achieved at RT. This superior performance of the binary electrolyte at 60 °C can be attributed to the synergistic effect of DMSO and IL. The addition of IL assists in the suppression of the evaporation rate of binary electrolytes when subjected to higher temperatures as shown in evaporation tests.

Furthermore, the discharge voltage plateau of the binary electrolyte is comparable with DMSO, unlike IL, irrespective of operating temperature. For the binary electrolyte, the discharge and charge voltage hysteresis decrease from 1.46 V to 1.08 V when the operating temperature increases from RT to 60 °C. This is attributed to the enhanced oxidation and reduction reaction rates with temperature, as confirmed in CV tests (Fig. 3b).

3.2.3. Evolution of Li_2O_2 morphology with temperature

The main discharge product of LOBs is Li_2O_2 which deposits on a porous cathode. Several different kinds of Li_2O_2 morphologies have been reported in the literature after examination of the deeply discharged cathode. These morphologies include toroidal-shaped, spherical particles, rod-like particles, thin films, and porous ball-like structures [54]. Various factors affect the morphology of the discharge product, including current density, the reaction mechanism of the formation of Li_2O_2 (disproportionation or electrochemical reduction), and operating temperatures. How discharge product accumulates on the cathode surface substantially impacts the overall battery performance. We studied the evolution of Li_2O_2 morphology with operating temperature using the binary electrolyte. Fig. 5 shows the SEM images of pristine and discharged cathodes to the fixed capacity of 1.0 Ah g^{-1} at 20 °C, 40 °C, and 60 °C. Fig. 5a shows the uncycled, pristine Vulcan XC cathode. At RT (Fig. 5b), Li_2O_2 is deposited in the form of disk-shaped particles. This type of morphology is common with DMSO electrolyte (as 80 vol% is DMSO), which exhibits a high Gutmann DN (29.8 kcal mol^{-1} [4]). The higher DN promotes the disproportionation of intermediate product LiO_2 to form Li_2O_2 in the form of big toroid-shaped particles [55].

At 40 °C (Fig. 5c), the Li_2O_2 deposited in the form of sphere-like particles. The size of the discharge product obtained at 40 °C is smaller than the one obtained at RT. At 60 °C (Fig. 5d), the morphology of the discharge product changed drastically from particle to uniform film-like morphology. The nucleation of Li_2O_2 initiates with the discharge process, followed by its growth as the discharge cycle continues. At lower operating temperatures, the number of nucleation sites is limited due to the large energy barrier, which promotes the formation of discharge products in bigger particles. The increased operating temperature reduces the energy barrier for nucleation, which gives rise to more nucleation sites on the cathode surface. As the number of nucleation sites increases, the discharge product size decreases. Besides

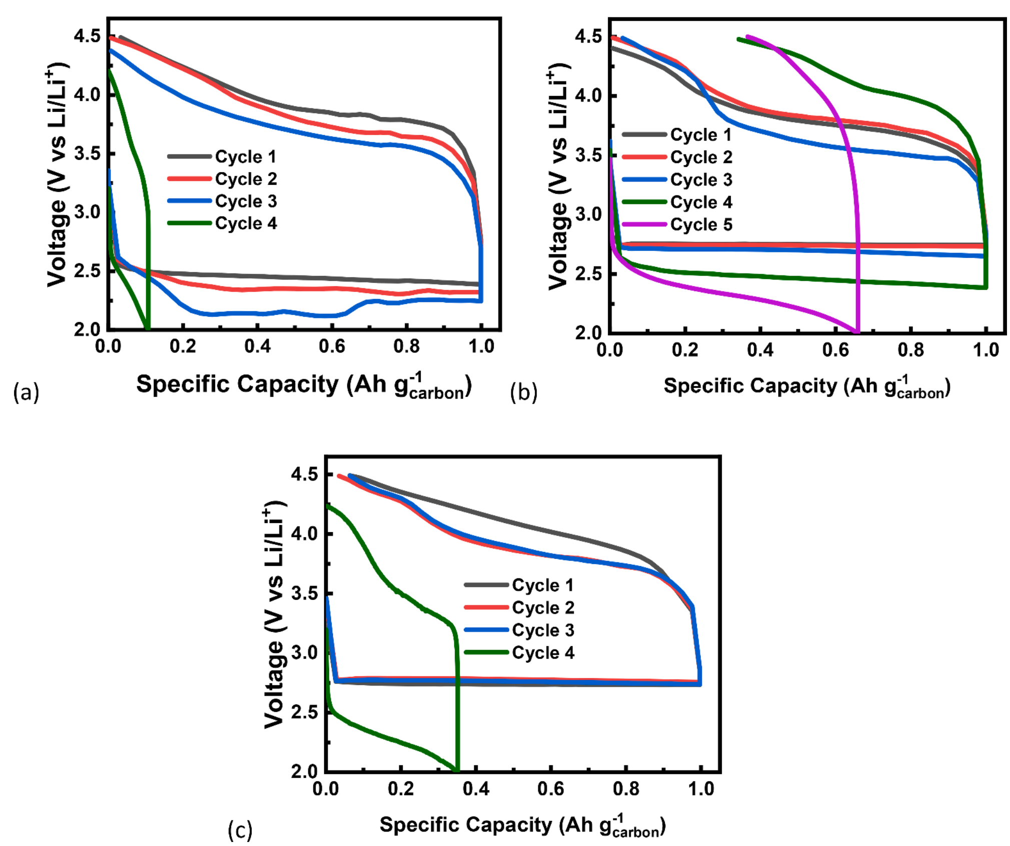

Fig. 7. Cycling stability plots of LOB at RT (20 °C) with **(a)** 0.5 M LiTFSI-[C_2C_1*im*][Tf_2N] **(b)** 0.5 M LiTFSI-[C_2C_1*im*][Tf_2N]/DMSO (1:4) and **(c)** 0.5 M LiTFSI-DMSO at current density of 0.1 mA cm^{-2}.

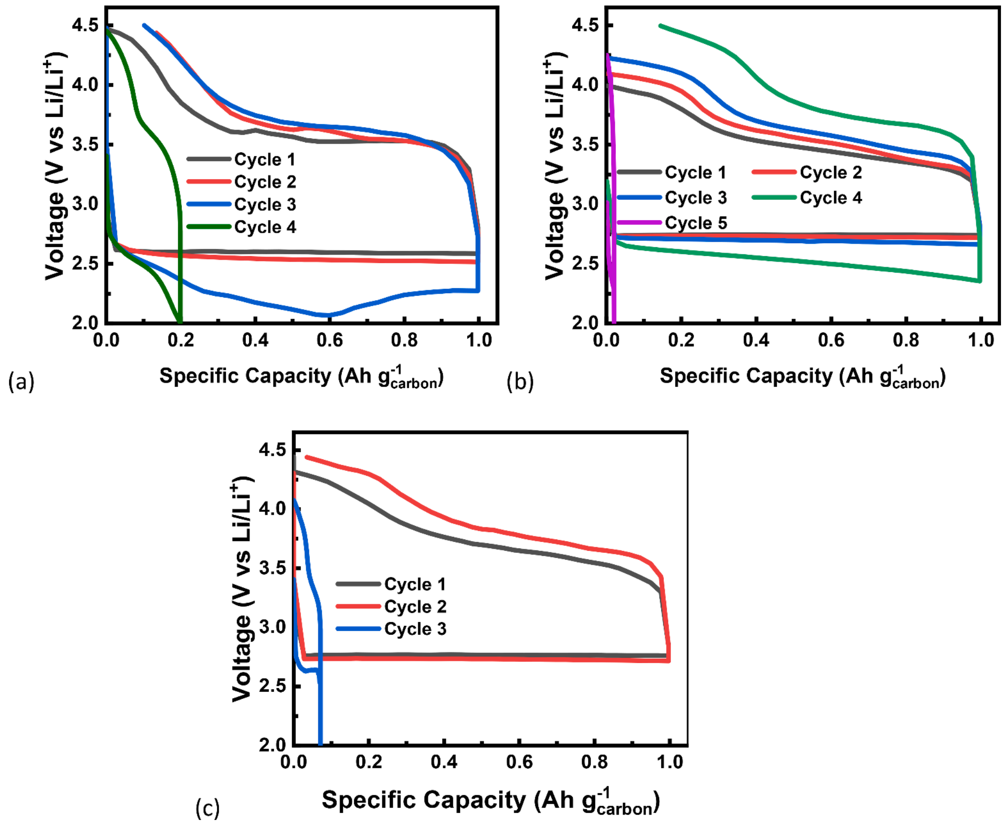

Fig. 8. Cycling stability plots of LOB at 40 °C with **(a)** 0.5 M LiTFSI-[C_2C_1*im*][Tf_2N] **(b)** 0.5 M LiTFSI-[C_2C_1*im*][Tf_2N]/DMSO (1:4) and **(c)** 0.5 M LiTFSI-DMSO at current density of 0.1 mA cm^{-2}.

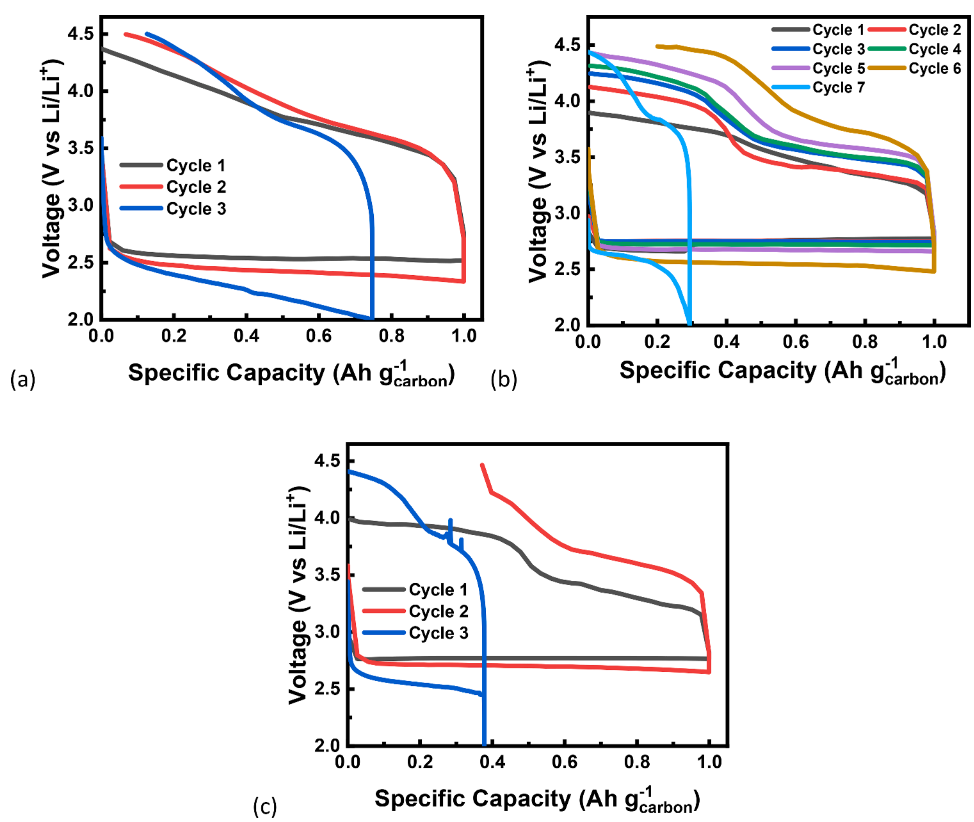

Fig. 9. Cycling stability plots of LOB at 60 °C with **(a)** 0.5 M LiTFSI-[C_2C_1*im*][Tf_2N] **(b)** 0.5 M LiTFSI-[C_2C_1*im*][Tf_2N]/DMSO (1:4) and **(c)** 0.5 M LiTFSI-DMSO at current density of 0.1 mA cm^{-2}.

nucleation sites, due to the higher mass transfer rate of electrochemical species at elevated temperatures, the discharge product accumulates more uniformly [21].

The composition of discharge product was examined by *ex-situ* XPS analysis. Fig. 6 shows the binding energy curves of Li 1 s, O 1 s and C 1 s spectra of pristine and discharged cathode samples at different temperatures. The pristine sample showed no peak for Li 1 s and a diminished peak for O 1s at 531 eV. However, a significant peak appeared in C 1s spectrum for C-C bond.

The binding energy peaks for Li_2O_2 are summarized in Table 3. At 20 °C and 40 °C, Li 1 s shows peaks at 54.9 eV and 54.95 eV, respectively. At 60 °C, the binding energy peak slightly shifted to 54.72 eV The binding energy peaks obtained for Li 1 s and O 1 s are also in good agreement for Li_2O_2 with the previous reports [56–59]. The presence of Li_2CO_3 was not detected for the sample discharged at RT. However, in C 1 s spectrum, a diminished peak appeared at 290 eV for the high temperature samples which corresponds to the presence of Li_2CO_3 [60].This could be ascribed to the thermal instability of Li_2O_2 at higher temperatures as reported in previous studies [61]. Furthermore, the discharged cathode (20 °C) was also analyzed under Raman Spectroscopy. Fig. S7 shows the comparison of Raman Spectra of fresh and discharged electrode. For discharged electrode, a pronounced peak appeared at 750 cm^{-1} which confirms the formation of Li_2O_2 during discharge cycle [62].

3.2.4. *Cycling stability*

Cycling stability tests were conducted with IL and DMSO pure electrolytes and IL/DMSO (1:4) binary electrolyte at 20 °C, 40 °C, and 60 °C. The specific capacity for all the tests was kept at 1.0 Ah g^{-1}. Fig. 7 shows the cycling stability results of the above-mentioned electrolytes at 20 °C. The binary electrolyte displays superior performance by yielding four cycles (Fig. 7b). On the other hand, both IL and DMSO yield three cycles lagging behind the binary electrolyte. The voltage gap for IL (~1.48 V) is noticeably higher than DMSO (~1.17 V). This could be ascribed to its high mass transfer resistance (due to high viscosity) and relatively high current density. Both the binary electrolyte and DMSO exhibit a high discharge voltage plateau and a low charge voltage plateau.

Fig. 8 shows the discharge/charge cycling stability plots with all three electrolytes obtained at 40 °C. The binary electrolyte maintained superior stability by yielding four cycles (Fig. 8b) followed by IL with three cycles (Fig. 8a) and DMSO, which incurs only two cycles.

Both discharge and charge voltage plateau improved substantially for IL. It is interesting to note that IL performs better than DMSO despite exhibiting high viscosity and low diffusivity of electrochemical species than its counterpart. This indicates that other parameters besides mass transport take into effect at elevated operating temperatures. High evaporation rates and reduced O_2 solubility in organic solvent can limit the battery performance in general.

Fig. 9 shows the discharge/charge cycling stability profiles of electrolytes under consideration. The binary electrolyte yields six cycles followed by pure electrolytes with two cycles each. The cycling performance of LOB with pure electrolytes deteriorated further at 60 °C, especially for IL. This could be ascribed to lower deep discharge capacity (Fig. 4c) yielded by these electrolytes at 60 °C, possibly due to further surge in evaporation rates of DMSO, lower oxygen solubility and degradation. Furthermore, the instability of IL in the presence of highly reactive superoxide radical and reduction of free DMSO molecules on Li surface exacerbates the battery cycling [63,64]. Unlike pure electrolytes, the LOB with binary electrolytes displayed an improvement in the number of cycles due to synergistic effects of IL/DMSO which results into alleviation of aforementioned factors.

The possible reason for this could be the accumulation of discharge product in the form of uniform film at higher operating temperatures (Fig. 5c). The charge potential required to disintegrate Li_2O_2 when deposited in a uniform film will be lower than Li_2O_2 toroids. This prevents the premature degradation of electrolytes and, consequently, the cell failure.

It is worth-mentioning that the voltage gap between discharge and charge cycles decreased with the increased temperature for all electrolytes, which depicts the improvement of the mass transport of ions. This further confirms the enhanced electrochemical activity at elevated temperatures as demonstrated by CV tests. Especially for binary electrolyte, the increased number of cycles at 60 °C can also be attributed to its faster kinetics as shown in Fig. 3b. Fig. S7 compares the average discharge and charge voltages of cycling stability tests with IL/DMSO (1:4) at various temperatures.

It is worth mentioning that the overall cycling performance of LOB with these electrolytes is not exceptional in this study due to other factors such as instability of Li anode and incorporation of Vulcan XC as carbon cathode without the further treatment with metal catalysts known for improving cycling stability. Nonetheless, irrespective of operating temperature, IL/DMSO (1:4) binary electrolyte has demonstrated superior cycling stability due to the synergistic effect of IL and DMSO.

4. Conclusion

We presented the influence of operating temperature on the electrochemical performance of LOB employing DMSO, $[C_2C_1im][Tf_2N]$, and $[C_2C_1im][Tf_2N]$/DMSO (1:4) binary electrolyte. LOB with binary electrolyte delivered the most stable performance by yielding 3.70 Ah g^{-1}, 4.0 Ah g^{-1}, and 3.65 Ah g^{-1} discharge capacities at 20 °C, 40 °C, and 60 °C, respectively. Furthermore, the superior stability of binary electrolytes at any given temperature was confirmed in cycling stability tests. Regardless of operating temperature (20 °C, 40 °C, 60 °C), the $[C_2C_1im][Tf_2N]$/DMSO (1:4) binary electrolyte yielded the highest ionic conductivity and low viscosity (comparable with DMSO) among other electrolytes. CV tests revealed significantly higher reaction rates for blended electrolyte as compared with neat electrolytes and displayed enhancement of ORR and OER with temperature. We observed the evolution of Li_2O_2 morphology with operating temperature in binary electrolyte. As the temperature increases, the discharge product deposition becomes more uniform, especially at 60 °C. Enhanced stability against superoxide ions, increased ionic conductivity, low viscosity, improved oxygen solubility, and suppressed evaporation rates are the major contributing factors to the superior performance of $[C_2C_1im][Tf_2N]$/DMSO (1:4) binary electrolyte.

CRediT authorship contribution statement

Syed Shoaib Hassan Zaidi: Methodology, Investigation, Software, Data curation, Writing – original draft. **Rajkumar Kore:** Methodology, Writing – review & editing. **Mark B. Shiflett:** Methodology, Writing – review & editing. **Xianglin Li:** Conceptualization, Supervision, Funding acquisition, Writing – review & editing.

Declaration of Competing Interest

The authors declare that they have no known competing financial interests or personal relationships that could have appeared to influence the work reported in this paper.

Data availability

Data will be made available on request.

Acknowledgements

The authors highly appreciate the support from the National Science Foundation (Awards 1941083).

Supplementary materials

Supplementary material associated with this article can be found, in the online version, at doi:10.1016/j.electacta.2023.143494.

References

[1] F. Wang, X. Li, X. Hao, J. Tan, Review and recent advances in mass transfer in positive electrodes of aprotic Li-O_2 batteries, ACS Appl. Energy Mater. 3 (3) (2020) 2258–2270, https://doi.org/10.1021/acsaem.9b02237. Mar.

[2] S.S.H. Zaidi, X. Li, Effects of oxygen cathode substrates with various carbon catalysts on the discharge capacity of lithium-oxygen battery, ECS Meet. Abs. MA2021-01 (6) (2021) 350, https://doi.org/10.1149/MA2021-016350mtgabs.

[3] S.S.H. Zaidi, X. Li, Li–O2/Air batteries using ionic liquids – a comprehensive review, Adv. Energy Mater. 13 (28) (2023), 2300985, https://doi.org/10.1002/aenm.202300985. Jul.

[4] S.S. Hassan Zaidi, S. Sigdel, C.M. Sorensen, G. Kwon, X. Li, Incorporation of novel graphene nanosheet materials as cathode catalysts in Li–O2 battery, J. Electrochem. Energy Conver. Storage 20 (2) (2023), https://doi.org/10.1115/1.4056937. May.

[5] F. Wang, P.K. Kahol, R. Gupta, X. Li, Experimental studies of carbon electrodes with various surface area for Li-O_2 batteries, J. Electrochem. Energy Conver. Storage 16 (4) (2019), https://doi.org/10.1115/1.4043229. Nov.

[6] K.M. Abraham, Z. Jiang, A polymer electrolyte-based rechargeable lithium/oxygen battery, J. Electrochem. Soc. 143 (1) (1996) 1, https://doi.org/10.1149/1.1836378.

[7] V. Esfahanian, M.T. Dalakeh, N. Aghamirzaie, Mathematical modeling of oxygen crossover in a lithium-oxygen battery, Appl. Energy 250 (2019) 1356–1365, https://doi.org/10.1016/j.apenergy.2019.04.124. Sep.

[8] S.S.H. Zaidi, X. Li, Comparing the electrochemical performance of organic and ionic liquid-based electrolytes in lithium-oxygen battery, ECS Meet. Abs. MA2021-02 (1) (2021) 144, https://doi.org/10.1149/MA2021-021144mtgabs.

[9] H. Guo, W. Luo, J. Chen, S. Chou, H. Liu, J. Wang, Review of electrolytes in nonaqueous lithium–oxygen batteries, Adv. Sustain. Syst. 2 (8–9) (2018), https://doi.org/10.1002/adsu.201700183. Wiley-VCH VerlagAug. 01.

[10] B.D. McCloskey, D.S. Bethune, R.M. Shelby, G. Girishkumar, A.C. Luntz, Solvents critical role in nonaqueous Lithium-Oxygen battery electrochemistry, J. Phys. Chem. Lett. 2 (10) (2011) 1161–1166, https://doi.org/10.1021/jz200352v. May.

[11] W. Xu, et al., The stability of organic solvents and carbon electrode in nonaqueous Li-O_2 batteries, J. Power Sources 215 (2012) 240–247, https://doi.org/10.1016/j.jpowsour.2012.05.021. Oct.

[12] S.A. Freunberger, et al., Reactions in the rechargeable lithium-O2 battery with alkyl carbonate electrolytes, J. Am. Chem. Soc. 133 (20) (2011) 8040–8047, https://doi.org/10.1021/ja2021747. May.

[13] J. Lai, Y. Xing, N. Chen, L. Li, F. Wu, R. Chen, Elektrolyte für wiederaufladbare Lithium-Luft-Batterien, Angew. Chem. 132 (8) (2020) 2994–3019, https://doi.org/10.1002/ange.201903459. Feb.

[14] T. Zhang, Z.-Y. Wen, A high-rate ionic liquid Lithium-O2 battery with LiOH product, J. Phys. Chem. C 121 (11) (2017) 5968–5973, https://doi.org/10.1021/acs.jpcc.7b00336. Mar.

[15] J. Zeng, C. Francia, J. Amici, S. Bodoardo, N. Penazzi, A highly reversible Li-O_2 battery utilizing a mixed electrolyte and a cathode incorporating Co_3O_4, RSC Adv. 5 (101) (2015) 83056–83064, https://doi.org/10.1039/c5ra13483h. Sep.

[16] E. Knipping, C. Aucher, G. Guirado, L. Aubouy, Suitability of blended ionic liquid-dimethylsulfoxide electrolyte for lithium-oxygen battery, Batter. Supercaps 2 (3) (2019) 200–204, https://doi.org/10.1002/batt.201800078. Mar.

[17] M. Asadi, et al., A lithium-oxygen battery with a long cycle life in an air-like atmosphere, Nature 555 (7697) (2018) 502–506, https://doi.org/10.1038/nature25984. Mar.

[18] S. Ferrari, et al., Investigation of ether-based ionic liquid electrolytes for Lithium-O2 batteries, J. Electrochem. Soc. 162 (2) (2015) A3001–A3006, https://doi.org/10.1149/2.0011502jes.

[19] A. Khan, C. Zhao, Enhanced performance in mixture DMSO/ionic liquid electrolytes: toward rechargeable Li-O_2 batteries, Electrochem. Commun. 49 (2014) 1–4, https://doi.org/10.1016/j.elecom.2014.09.014.

[20] L. Cecchetto, M. Salomon, B. Scrosati, F. Croce, Study of a Li-air battery having an electrolyte solution formed by a mixture of an ether-based aprotic solvent and an ionic liquid, J. Power Sources 213 (2012) 233–238, https://doi.org/10.1016/j.jpowsour.2012.04.038. Sep.

[21] P. Tan, W. Shyy, T.S. Zhao, Z.H. Wei, L. An, Discharge product morphology versus operating temperature in non-aqueous lithium-air batteries, J. Power Sources 278 (2015) 133–140, https://doi.org/10.1016/j.jpowsour.2014.12.049. Mar.

[22] J.B. Park, et al., Influence of temperature on lithium-oxygen battery behavior, Nano Lett. 13 (6) (2013) 2971–2975, https://doi.org/10.1021/nl401439b. Jun.

[23] K. Yoo, A.M. Dive, S. Kazemiabnavi, S. Banerjee, P. Dutta, Effects of operating temperature on the electrical performance of a li-air battery operated with ionic liquid electrolyte, Electrochim. Acta 194 (2016) 317–329, https://doi.org/10.1016/j.electacta.2016.02.099. Mar.

[24] S. Monaco, F. Soavi, M. Mastragostino, Role of oxygen mass transport in rechargeable Li/O2 batteries operating with ionic liquids, J. Phys. Chem. Lett. 4 (9) (2013) 1379–1382, https://doi.org/10.1021/jz4006256. May.

[25] L.T. Costa, B. Sun, F. Jeschull, D. Brandell, Polymer-ionic liquid ternary systems for Li-battery electrolytes: molecular dynamics studies of LiTFSI in a EMIm-TFSI and PEO blend, J. Chem. Phys. 143 (2) (2015), https://doi.org/10.1063/1.4926470. Jul.

[26] U. Ulissi, et al., Low-polarization lithium–oxygen battery using [DEME][TFSI] ionic liquid electrolyte, ChemSusChem 11 (1) (2018) 229–236, https://doi.org/10.1002/cssc.201701696. Jan.

[27] S.K. Das, S. Xu, A.-H. Emwas, Y.Y. Lu, S. Srivastava, L.A. Archer, High energy lithium–oxygen batteries – transport barriers and thermodynamics, Energy Environ. Sci. 5 (10) (2012) 8927–8931, https://doi.org/10.1039/C2EE22470D.

[28] M.S. Alam, B. Ashokkumar, A.M. Siddiq, The density, dynamic viscosity and kinematic viscosity of protic and aprotic polar solvent (pure and mixed) systems: an experimental and theoretical insight of thermophysical properties, J. Mol. Liq. 281 (2019) 584–597, https://doi.org/10.1016/j.molliq.2019.02.097. May.

[29] H. Matsumoto, M. Yanagida, K. Tanimoto, M. Nomura, Y. Kitagawa, Y. Miyazaki, Highly Conductive Room Temperature Molten Salts Based on Small Trimethylalkylammonium Cations and Bis(trifluoromethylsulfonyl)imide, Chem. Lett. 29 (8) (2000) 922–923, https://doi.org/10.1246/cl.2000.922. Aug.

[30] C. Comminges, R. Barhdadi, M. Laurent, M. Troupel, Determination of viscosity, ionic conductivity, and diffusion coefficients in some binary systems: ionic liquids + molecular solvents, J. Chem. Eng. Data 51 (2) (2006) 680–685, https://doi.org/10.1021/je0504515. Mar.

[31] S.S. Moganty, R.E. Baltus, Regular solution theory for low pressure carbon dioxide solubility in room temperature ionic liquids: ionic liquid solubility parameter from activation energy of viscosity, Ind. Eng. Chem. Res. 49 (12) (2010) 5846–5853, https://doi.org/10.1021/ie901837k. Jun.

[32] D. Zigah, A. Wang, C. Lagrost, P. Hapiot, Diffusion of molecules in ionic liquids/organic solvent mixtures. Example of the reversible reduction of O2 to superoxide, J. Phys. Chem. B 113 (7) (2009) 2019–2023, https://doi.org/10.1021/jp8095314. Feb.

[33] P.H. Reinsberg, P.P. Bawol, E. Thome, H. Baltruschat, Fast and simultaneous determination of gas diffusivities and solubilities in liquids employing a thin-layer cell coupled to a mass spectrometer, Part II: proof of concept and experimental results, Anal. Chem. 90 (24) (2018) 14150–14155, https://doi.org/10.1021/acs.analchem.8b04320. Dec.

[34] H. Gupta, et al., Effect of temperature on electrochemical performance of ionic liquid based polymer electrolyte with Li/LiFePO4 electrodes, Solid State Ion 309 (2017) 192–199, https://doi.org/10.1016/j.ssi.2017.07.019. Oct.

[35] K. Tochigi, H. Yamamoto, Estimation of ionic conductivity and viscosity of ionic liquids using a QSPR model, J. Phys. Chem. C 111 (43) (2007) 15989–15994, https://doi.org/10.1021/jp073839a. Nov.

[36] A. Heist, S.-H. Lee, Improved stability and rate capability of ionic liquid electrolyte with high concentration of LiFSI, J. Electrochem. Soc. 166 (10) (2019) A1860–A1866, https://doi.org/10.1149/2.0381910jes.

[37] P. Tan, Z. Wei, W. Shyy, T.S. Zhao, Prediction of the theoretical capacity of non-aqueous lithium-air batteries, Appl. Energy 109 (2013) 275–282, https://doi.org/10.1016/j.apenergy.2013.04.031.

[38] C.O. Laoire, S. Mukerjee, K.M. Abraham, E.J. Plichta, M.A. Hendrickson, Influence of nonaqueous solvents on the electrochemistry of oxygen in the rechargeable lithium-air battery, J. Phys. Chem. C 114 (19) (2010) 9178–9186, https://doi.org/10.1021/jp102019y. May.

[39] J.N. Canongia Lopes, et al., Polarity, viscosity, and ionic conductivity of liquid mixtures containing [C4C1im][Ntf2] and a molecular component, J. Phys. Chem. B 115 (19) (2011) 6088–6099, https://doi.org/10.1021/jp2012254. May.

[40] T.-Y. Wu, et al., Diffusion coefficients, spin-lattice relaxation times, and chemical shift variations of NMR spectra in LiTFSI-doped ether- and allyl-functionalized dicationic ionic liquids, J. Taiwan Inst. Chem. Eng. 60 (2016) 138–150, https://doi.org/10.1016/j.jtice.2015.10.047.

[41] O. Nordness, J.F. Brennecke, Ion dissociation in ionic liquids and ionic liquid solutions, Chem. Rev. 120 (23) (2020) 12873–12902, https://doi.org/10.1021/acs.chemrev.0c00373. American Chemical SocietyDec. 09.

[42] N.A. Galiote, S. Jeong, W.G. Morais, S. Passerini, F. Huguenin, The role of ionic liquid in oxygen reduction reaction for lithium-air batteries, Electrochim. Acta 247 (2017) 610–616, https://doi.org/10.1016/j.electacta.2017.06.137.

[43] F. de Giorgio, F. Soavi, M. Mastragostino, Effect of lithium ions on oxygen reduction in ionic liquid-based electrolytes, Electrochem. Commun. 13 (10) (2011) 1090–1093, https://doi.org/10.1016/j.elecom.2011.07.004.

[44] A. Khan, C. Zhao, Oxygen reduction reactions in aprotic ionic liquids based mixed electrolytes for high performance of Li–O2 batteries, ACS Sustain. Chem. Eng. 4 (2) (2016) 506–513, https://doi.org/10.1021/acssuschemeng.5b00890. Feb.

[45] C.J. Allen, et al., Oxygen reduction reactions in ionic liquids and the formulation of a general ORR mechanism for Li–Air batteries, J. Phys. Chem. C 116 (39) (2012) 20755–20764, https://doi.org/10.1021/jp306718v. Oct.

[46] C.J. Allen, S. Mukerjee, E.J. Plichta, M.A. Hendrickson, K.M. Abraham, Oxygen electrode rechargeability in an ionic liquid for the Li–Air battery, J. Phys. Chem. Lett. 2 (19) (2011) 2420–2424, https://doi.org/10.1021/jz201070t. Oct.

[47] S. Monaco, A.M. Arangio, F. Soavi, M. Mastragostino, E. Paillard, S. Passerini, An electrochemical study of oxygen reduction in pyrrolidinium-based ionic liquids for lithium/oxygen batteries, Electrochim. Acta 83 (2012) 94–104, https://doi.org/10.1016/j.electacta.2012.08.001.

[48] J.A. Choi, E.G. Shim, B. Scrosati, D.W. Kim, Mixed electrolytes of organic solvents and ionic liquid for rechargeable lithium-ion batteries, Bull. Korean Chem. Soc. 31 (11) (2010) 3190–3194, https://doi.org/10.5012/bkcs.2010.31.11.3190. Nov.

[49] L.T.M. Le, et al., Mixing ionic liquids and ethylene carbonate as safe electrolytes for lithium-ion batteries, J. Mol. Liq. 271 (2018) 769–777, https://doi.org/10.1016/j.molliq.2018.09.068.

[50] T. Song, O. Morales-Collazo, J.F. Brennecke, Solubility and diffusivity of oxygen in ionic liquids, J. Chem. Eng. Data 64 (11) (2019) 4956–4967, https://doi.org/10.1021/acs.jced.9b00750. Nov.

[51] B.-C. Lee, S.L. Outcalt, Solubilities of gases in the ionic Liquid 1- n -Butyl-3-methylimidazolium Bis(trifluoromethylsulfonyl)imide, J. Chem. Eng. Data 51 (3) (2006) 892–897, https://doi.org/10.1021/je050357o. May.

[52] W. Xu, J. Xiao, J. Zhang, D. Wang, J.-G. Zhang, Optimization of nonaqueous electrolytes for primary lithium/air batteries operated in ambient environment, J. Electrochem. Soc. 156 (10) (2009) A773, https://doi.org/10.1149/1.3168564.

[53] B. Garcia, S. Lavallée, G. Perron, C. Michot, M. Armand, Room temperature molten salts as lithium battery electrolyte, Electrochim. Acta 49 (26) (2004) 4583–4588, https://doi.org/10.1016/j.electacta.2004.04.041. Oct.

[54] Z. Ma, et al., A review of cathode materials and structures for rechargeable lithium-air batteries, Energy and Environmental Science 8 (8) (2015) 2144–2198, https://doi.org/10.1039/c5ee00838g. Royal Society of Chemistry.

[55] M. Zhu, et al., Direct observation of solvent donor number effect on lithium-oxygen battery capacity via a nanoarray cathode model, J. Phys. Chem. C 126 (25) (2022) 10248–10257, https://doi.org/10.1021/acs.jpcc.2c01211. Jun.

[56] J. Li, et al., Polarized nucleation and efficient decomposition of Li_2O_2 for Ti_2C MXene cathode catalyst under a mixed surface condition in lithium-oxygen batteries, Energy Storage Mater. 35 (2021) 669–678, https://doi.org/10.1016/j.ensm.2020.12.004. Elsevier B.V.Mar. 01.

[57] R. Younesi, S. Urbonaite, K. Edström, M. Hahlin, The cathode surface composition of a cycled $Li-O_2$ battery: a Photoelectron spectroscopy study, J. Phys. Chem. C 116 (39) (2012) 20673–20680, https://doi.org/10.1021/jp302168h. Oct.

[58] R. Younesi, M. Hahlin, F. Björefors, P. Johansson, K. Edström, $Li-O_2$ battery degradation by lithium peroxide (Li 2O2): a model study, Chem. Mater. 25 (1) (2013) 77–84, https://doi.org/10.1021/cm303226g. Jan.

[59] S.S. Hassan Zaidi, S. Rajendran, A. Sekar, A. Elangovan, J. Li, X. Li, Binder-free $Li-O_2$ battery cathodes using Ni- and PtRu-coated vertically aligned carbon nanofibers as electrocatalysts for enhanced stability, Nano Res. Energy (2023) 1–11, https://doi.org/10.26599/NRE.2023.9120055. Feb.

[60] D. Aurbach, et al., XPS Analysis of Lithium Surfaces Following Immersion in Various Solvents Containing LiBF 4 XPS Analysis of Lithium Surfaces Following Immersion in Various Solvents Containing LiBF4, Pergamon Press, 1995.

[61] K.P.C. Yao, et al., Thermal stability of Li_2O_2 and Li_2O for Li-Air batteries: in Situ XRD and XPS studies, J. Electrochem. Soc. 160 (6) (2013) A824–A831, https://doi.org/10.1149/2.069306jes.

[62] Y. Yang et al., 'Supporting information tuning the morphology and crystal structure of Li2O2—a graphene model electrode study for Li-O2 battery'.

[63] M. Hayyan, M.A. Hashim, I.M. Alnashef, Superoxide ion: generation and chemical implications, Chem. Rev. 116 (5) (2016) 3029–3085, https://doi.org/10.1021/acs.chemrev.5b00407. American Chemical SocietyMar. 09.

[64] A.R. Neale, et al., Design parameters for ionic liquid–molecular solvent blend electrolytes to enable stable Li metal cycling within $Li–O_2$ batteries, Adv. Funct. Mater. 31 (27) (2021), https://doi.org/10.1002/adfm.202010627. Jul.